Copyright ⓒ2017 KSII

Analytical Evaluation of FFR-aided Heterogeneous Cellular Networks with Optimal Double Threshold

Sani Umar Abdullahi, Jian Liu and Seyed Alireza Mohadeskasaei
School of Computer and Communications Engineering, University of Science and Technology Beijing, Beijing 100083 - P.R.China.
[e-mail: saniumar.a.ng@ieee.org, liujian@ustb.edu.cn, alireza.kasaee@gmail.com]
*Corresponding Author: Sani Umar Abdullahi

Received January 16, 2017; revised March 22, 2017; accepted April 9, 2017; published July 31, 2017

Abstract

Next Generation Beyond 4G/5G systems will rely on the deployment of small cells over conventional macrocells for achieving high spectral efficiency and improved coverage performance, especially for indoor and hotspot environments. In such heterogeneous networks, the expected performance gains can only be derived with the use of efficient interference coordination schemes, such as Fractional Frequency Reuse (FFR), which is very attractive for its simplicity and effectiveness. In this work, femtocells are deployed according to a spatial Poisson Point Process (PPP) over hexagonally shaped, 6-sector macro base stations (MeNBs) in an uncoordinated manner, operating in hybrid mode. A newly introduced intermediary region prevents cross-tier, cross-boundary interference and improves user equipment (UE) performance at the boundary of cell center and cell edge. With tools of stochastic geometry, an analytical framework for the signal-to-interference-plus-noise-ratio (SINR) distribution is developed to evaluate the performance of all UEs in different spatial locations, with consideration to both co-tier and cross-tier interference. Using the SINR distribution framework, average network throughput per tier is derived together with a newly proposed harmonic mean, which ensures fairness in resource allocation amongst all UEs. Finally, the FFR network parameters are optimized for maximizing average network throughput, and the harmonic mean using a fair resource assignment constraint. Numerical results verify the proposed analytical framework, and provide insights into design trade-offs between maximizing throughput and user fairness by appropriately adjusting the spatial partitioning thresholds, the spectrum allocation factor, and the femtocell density.

***Keywords*:** Heterogeneous networks, Fractional Frequency Reuse, Stochastic Geometry, SINR distribution, Throughput, Harmonic mean

This work was supported by the National Major Project under Grant No. 2015ZX03001013-002.

https://doi.org/10.3837/tiis.2017.07.004 **ISSN : 1976-7277**

1. Introduction

1.1. Background

Due to the proliferation of increasingly intelligent mobile devices and the advent of machine communications and other bandwidth-hungry applications, existing mobile networks are quickly evolving from voice-based, homogeneous architectures to more diverse, heterogeneous and data-centric networks in order to cope with the exponential data demands and need for ubiquitous connectivity with improved user experience [1]. In traditional homogeneous networks, mobile users in indoor environments and those located far away from the macrocells often experience poor coverage and degraded user throughputs due to wall penetration losses and fading respectively. Advent of heterogeneous networks (Hetnets), which consist of various network tiers such as the operator deployed macrocells, picocells/relays and distributed antenna systems, together with end-user deployed femtocells, has led to significant increase in user signal-to-interference-plus-noise-ratio (SINR) by increasing the received signal strength due to decreased distance between receiver and transmitter through the use of cost-effective small cells.

Femtocells are low-power (10-100mw), short-range (10-30m), plug-and-play type access points operating in operators' licensed spectrum and connected to their own wired backhaul connections which have the capability of off-loading traffic from macrocells to serve indoor users with much improved network quality access in a cost-effective manner [2]. Home femtocells are usually deployed in an unplanned manner by end-users, mostly operating in co-channel mode to the macrocells for improved spectral utilization and avoiding high costs of spectrum licenses [3], or in orthogonal mode to the macrocells [4]. Each deployment mode has to trade one performance metric for another; interference for spectral efficiency (as in the former) and the reverse order for the latter. For security, economic reasons and backhaul limitations, many femtocells allow access to only authorized subscribers which are said to belong to a closed subscriber group (CSG), barring any other user equipments (UEs) irrespective of location or tier association. In such shared spectrum networks with closed access mode operation, cross-tier interference is particularly severe, especially for femto users (FUEs) in close proximity to the high-powered macrocells or macro users (MUEs) located indoors within coverage range of the femtocells. Such interference could completely degrade the entire network performance if no effective resource allocation and interference mitigation techniques are employed [5].

Recently, fractional frequency reuse (FFR) has emerged as an attractive intercell interference coordination technique for state-of-the-art orthogonal frequency division multiple access (OFDMA)-based cellular systems such as 3GPP long term evolution (LTE) and LTE-Advanced (LTE-A) due to its low implementation complexity and significant performance gains for cell edge users. In FFR, the entire spectrum is partitioned into multiple frequency divisions, such that user equipments (UEs) in close proximity to the macro base station or with good received signal quality are served with full-frequency reuse on a certain frequency partition, while other UEs located farther away are served with higher reuse factors on other bands to mitigate intercell interference. Hence, use of FFR leads to a trade-off between improving rate and coverage of cell edge users and overall network spectral efficiency[6]. Though the FFR framework was initially proposed for homogeneous macro networks to mitigate intercell interference (ICI), it could also be utilized in multi-tier networks for effective resource allocation and interference management by strategic spectrum

partitioning and resource sharing [7].

1.2. Recent work

Numerous works have recently employed FFR in two-tier networks of macro overlaid with femtocells for co-tier and cross-tier interference mitigation both in static and dynamic modes. Dynamic FFR schemes [8-10] are more resilient to uneven traffic bursts and network dynamics but are far more complex to implement and much less scalable than static schemes [11-15]. Authors in [11] propose a 6-sectored FFR scheme with effective cross-tier interference minimization, increased resource allocation to edge FUEs, and found via numerical simulation, the optimal network configurations that maximize total throughput. Bilios et al propose in [12] an adaptive mechanism using iterative simulations to determine the optimal FFR scheme which maximized user satisfaction and total throughput, while authors in [13] derive analytically the optimal signal-to-interference (SIR) thresholds which maximize coverage probability for both FFR and Soft Frequency Reuse (SFR) networks. Similarly in [14], a method for determining the partitioning criterion and amount of time resource for different cell regions is proposed to maximize average capacity and ensure fairness. Lastly, our previous work in [15] addressed a common cross-tier interference scenario for UEs located within the boundary of cell-center and cell-edge in two-tier macro/femto FFR-based OFDMA networks by providing an intermediary region where co-channel operation is avoided, while increasing resource share to MUEs in this buffer region.

However, all of the above listed studies relied on computer-intensive and time-consuming simulations for performance analysis of two-tier macro/femto OFDMA networks which are more personalized and very specific to defined environments, hence are usually incapable of conveying in-depth theoretical interpretations of performance metrics and insight to system design from the results easily. Recent research works exploit tools from stochastic geometry to analytically evaluate performance of both homogeneous networks [16-19] and Hetnets [20-22] where the locations of the macro base stations (MeNBs) and femto base stations (known as HeNBs in LTE-A) are assumed to be distributed according to a point process, usually the homogeneous Poisson point process (PPP) for its tractability. The methodology in [16, 17] has been quite instrumental in providing the foundation for analytical computations of key performance metrics characterized over the entire system, such as coverage and rate, from which most studies evaluating multi-tier networks with PPP were built [20-23]. However, it is critical for network providers to understand and analyze the performance for any given cell within the network and not simply on a system-wide measure as provided by previous stochastic geometry-based FFR studies. Hence, the authors in [21] improved the work in [16] by inscribing a fixed-size circular cell within the weighted voronoi tessellation hence enabling key performance insights to be obtained over the target cell using tools of stochastic geometry.

In reality, operators usually deploy macrocells upon careful provisioning and planning, for achieving cost-effective coverage and QoS targets, while femtocells being consumer deployed, are distributed with no planning or need for coordination/cooperation. Furthermore, performance of varying inter-cell interference coordination (ICIC) techniques such as FFR, use of directional antennas, and other interference reduction measures have been well studied and implemented under regular tessellations of macrocells. Hence, the authors in [24] employed stochastic geometry for modeling the random distribution of femtocells while the planned macrocells are modeled as deterministic hexagonal grid models with the objective of mitigating intercell and cross-tier interference via a spectrum swapping allocation for the femtocells, but with a limitation of neglecting the interference from neighbouring macrocells and small-scale fading in their analysis. The recent work in [25] addresses these limitations

and proposes an analytical framework for determining the optimal FFR parameters in the spatial and frequency domains under varying optimization criteria and scheduling policies. Authors in [26] propose a framework for analytically deriving the optimal spectrum allocation factor in macro/femto FFR network that could maximize long-term network throughput subject to some quality of service constraint. Differently than [24-26] however, this paper provides a novel analytical framework for performance evaluation of FFR-aided networks using PPP that is more compatible to modern practical deployments using directional antennas at the macrocell, without resorting to scenario-specific, extensive system-level simulations as in [8-14]. Furthermore, most previous FFR-works [8-14], [20], [24-26] do not address a severe cross-tier interference at the boundary of cell center and cell edge (referred to here as intermediary region) which could seriously degrade performance of both macro and femto UEs in this region. Lastly, a straight-forward mathematical concept called Harmonic mean is employed to improve equitable resource distribution in this work. Specific contributions of this work are hereby given in the following section.

1.3. Contributions and Structure

This research proposes an analytical scheme for evaluating the performance of OFDMA-based Hetnets utilizing FFR for interference mitigation and resource partitioning. Shared spectrum usage is employed between macro and femto networks, and there is no coordination between the two different tiers. The key contributions of this paper are summarized as thus:

- The combination of stochastic geometry tools for modeling random femtocells and a deterministic grid model for the hexagonally shaped macrocells allows for analytical performance evaluation, while preserving existing, efficient interference and capacity improvement mechanisms, such as FFR and the use of antenna sectorization.
- The effects of both co-tier and cross-tier interference are well investigated in this work, including at the boundary of cell-center and cell-edge regions, which is commonly ignored in most prior works. Using similar approach to our previous work in [15], we propose an intermediary region where spectrum sharing between femtocells and macro UEs is avoided for interference mitigation. A theoretical SINR distribution framework for the different kinds of UEs is then provided, which enables the derivation of per-tier coverage probability and average user throughputs provided by both macrocell and femtocell networks.
- Finally, we optimize the FFR-related parameters (the spatial partitioning thresholds R_m and R_f and spectrum allocation factor) that will maximize total network throughput and a new metric called the harmonic mean for ensuring fairness amongst all UEs. The effects of number of MUEs per cell, femtocell density and wall-partition losses on overall network throughput and optimization parameters are also investigated. The proposed analytical framework provides practical design guidelines for effective and interference-reduced femtocell deployments.

The rest of the paper is structured as follows: Section 2 provides the system model and insights into basic assumptions made to simplify the scheme for analytical tractability. Section 3 provides analytical framework for obtaining the coverage probability for the different kinds of UEs based on their spatial locations within the cell area, while Section 4 analyzes the throughput and harmonic mean realizations and the optimization scheme subject to varying performance restrictions. Section 5 presents the performance results while the paper is concluded in Section 6.

2. System Model

2.1 Network Topology

We consider the downlink of an OFDMA two-tier network using FFR where the macrocells are deployed after careful design and planning in a manner to cover the entire coverage area and hence could be modeled as regular tessellations of hexagonally shaped coverage areas with the macro base stations (MeNBs) located at the center of the hexagons. The entire network is made up of 19 macrocells in total, with the macrocell of interest, M_0 located at the origin $(0,0)$ of the R^2 plane with coverage area $|C|$, surrounded by 2 layers of neighbouring macrocells, where M_k, represents the k_{th} macrocell as shown in **Fig. 1(a)**. The first layer consists of 6 macrocells labeled (1-6) with the locations of M_k at (x_k, y_k), while the second layer consists of 12 macrocells (labeled 7-18) with the locations of M_k at (p_k, q_k) as given in (1) respectively. The inter-site distance is given by $\sqrt{3}R_C$, where R_C is the cell radius.

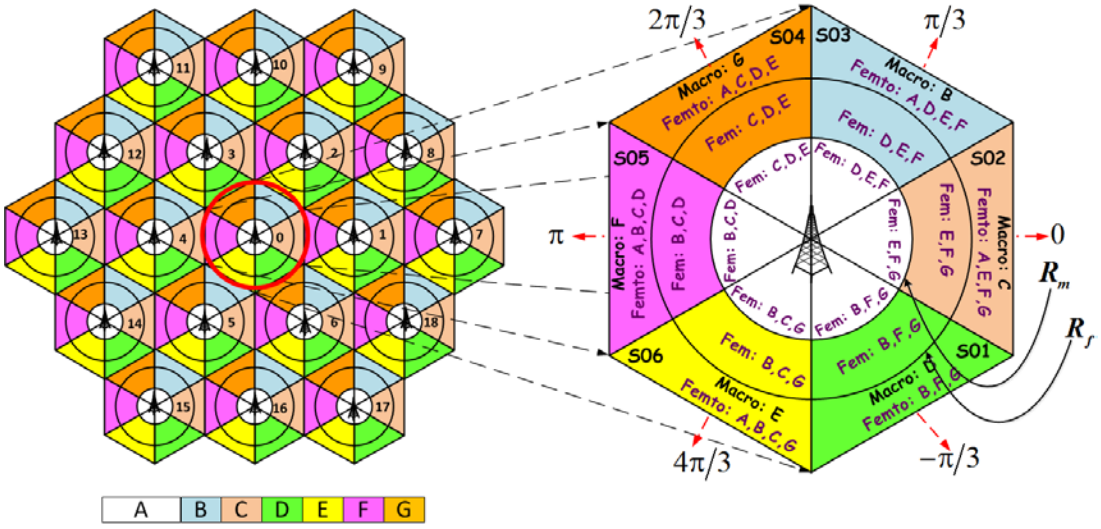

(a) **(b)**

Fig. 1. (a) Base Station Topology (b) Proposed macrocell structure showing main-beam pointing direction of each sector

$$M_k = \begin{cases} \sqrt{3}R_C \cos\left((k-1)\dfrac{\pi}{3}\right),\ \sqrt{3}R_C \sin\left((k-1)\dfrac{\pi}{3}\right) & k = 1:6 \quad \text{first layer} \\ 2\sqrt{3}R_C \cos\left((k-1)\dfrac{\pi}{6}\right),\ 2\sqrt{3}R_C \sin\left((k-1)\dfrac{\pi}{6}\right) & k = 7:18 \quad \text{second layer} \end{cases} \tag{1}$$

Based on the principle of static FFR to improve cell-edge users performance, the MUEs are partitioned into center region (CCR) and edge region (CER) respectively using the average received SINR measure, where the MeNB classifies MUEs with average received SINR less than the defined threshold as edge-UEs, while those with average received SINR greater than the threshold are cell-center UEs. An omnidirectional antenna is then employed in the CCR of all macrocells, while sixty-degree directional antennas are employed at the CER of all macrocells to partition the CER into six different non-overlapping, equal areas to minimize

interference and improve SINR. This scheme carves out a new intermediary region (CIR) from within the CER to further minimize cross-tier interference at the boundary as illustrated in **Fig. 2**. The extent of both the CCR radius and CIR are crucial design parameters that will be discussed in subsequent sections of the paper. For each macrocell M_k ($k \in \{0,1,2.....18\}$) there are six equal sectors: S_{k1}, S_{k2}….S_{k6} where the bore-sight of each S_{kl} ($l \in \{1,2,3,4,5,6\}$) is given by $\Upsilon_l = 2(l-2)\frac{\pi}{6}$ such that the arrangement of the sectors is as shown in **Fig. 1(b)**. Closed-access femtocells, each with radius R_{HeNB}, are distributed randomly over the entire cellular network in indoor environments according to a spatial Poisson Point Process (PPP) denoted by Ω_f with intensity λ_f . To avoid cross-tier interference, the femtocells in any macro coverage area do not use same frequency band with the macro UEs in that same region, but can share with MUEs of other regions.

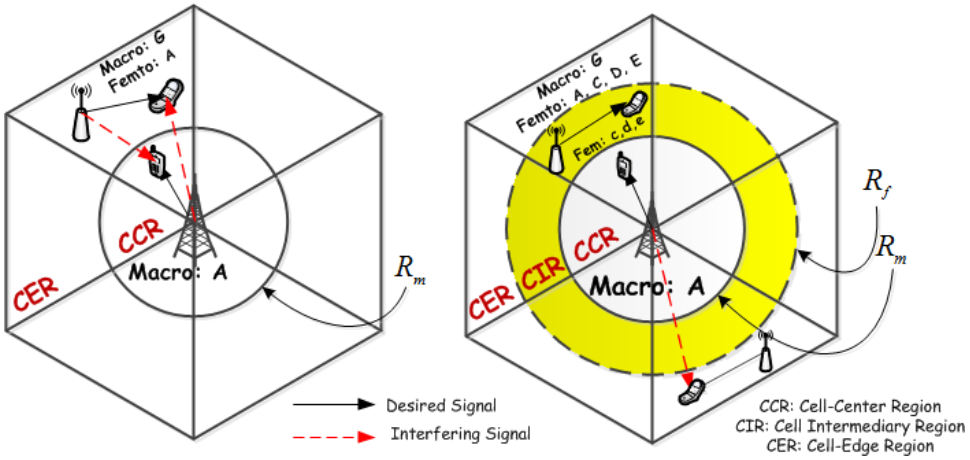

(a) Without Intermediary Region (b) With Intermediary Region

Fig. 2. Illustration of Interference Statistics with and without Intermediary Region

Fig. 2 gives insight to the effect of cross-tier interference at transition area of center and edge areas of a cell. In **Fig 2 (a)**, both MUEs and FUEs experience severe cross-tier interference when same spectrum is shared by both network tiers (i.e. Sub-band A), while by introducing a new intermediary region to avoid spectrum sharing at transition areas, the effect is minimized as shown in **Fig 2 (b)** similar to the method employed in this work.

2.2 Key Assumptions

The following key assumptions (AS) have been made in this work for the sake of analytical convenience:

AS1: The basic resource unit allocated to each user in OFDMA-based systems is the resource block (RB) whereby intracell interference is avoided by scheduling at most one user to one RB in each cell [27],[28] . Due to the restrictions of bandwidth and time duration of each RB according to the LTE standard, all subcarriers within the same RB are assumed to experience identical Rayleigh fading [29]. Subcarriers within the same RB also have equal power.

AS2: Channel blind Round Robin (RR) scheduling is assumed

AS3: The hexagonal macrocell of interest, M_0, is approximated as a disc which has the same area as the respective hexagon given as $|C| = \pi R_C^2$ as shown in **Fig. 1**. The radius of the

circular cell is given by $R_C = R_{Hex}\sqrt{\frac{3\sqrt{3}}{2\pi}}$ where R_{Hex} is the radius of the original hexagon [30].

AS4: Although in reality MUEs first measure received pilot signals to determine average received SINR which is used to classify cell-center and cell-edge UEs, for sake of tractability the partitioning criterion used in this work is a circular distance with radius R_m as shown in **Fig. 1** to separate the UEs in CCR and CER respectively. An intermediary radius R_f, is then used to classify FUEs as cell-center and cell-edge FUEs respectively, to avoid severe cross-tier interference at boundary of the two regions.

AS5: The spatial PPP distributed femtocells are denoted by Ω_f with intensity λ_f, where the mean number of femtocells per macrocell is given as $N_f = \lambda_f |C|$. Each femtocell is assumed to be of circular coverage region and in indoor environment, with the HeNB assumed to be deployed at the center of the cell with radius R_{HeNB}, using an omnidirectional antenna.

AS6: MUEs and FUEs are uniformly and independently distributed over the entire macro coverage area, with FUEs associated to respective HeNBs.

AS7: Due to the symmetric structure of the macrocell sectors, we provide analytical framework for one sector only for brevity, since similar results will be realized for other sectors. S_{03} of cell M_o is considered.

AS8: Lastly, for the analysis of FUE SINR or femto-macro interference, since $R_C >> R_{HeNB}$, we safely assume that the distance of the respective FUE to the interfering MeNB is approximately equal to the distance of the tagged HeNB of the FUE to the interfering MeNB.

2.3 Channel model and SINR

The downlink wireless channel model is comprised of path-loss (α) and small scale fading $g_u(G_\psi)$ between any base station ψ and the specific UE u, which is i.i.d (independent and identically distributed) exponentially distributed with mean μ (corresponding to Rayleigh fading) [20]. The wall penetration loss (ϑ) is considered for links penetrating walls such as indoor to outdoor or vice-versa, while a double wall penetration loss ϑ^2 is considered for indoor transmissions from one femto-cell to neighbouring indoor femto-cells/UEs. The instantaneous SINR of a UE u in the reference cell M_o on sub-carrier k of resource block n, (n_k), at a random distance from M_o, is given as;

$$SINR_u^{n_k} = \frac{P_{M_{0l,u}} g_u r^{-\alpha}}{\sigma^2 + I_u^{n_k}} \tag{2}$$

where r is the distance of the UE from M_o, $P_{M_{0l,u}}$ the transmit power per resource block of sector S_{0l}. g_u is the exponentially distributed channel power gain (Rayleigh fading), σ^2 is the additive noise power, while $I_u^{n_k}$ represents the total interference from both macrocells and femtocells and is given by;

$$I_u^{n_k} = I_M + I_{FM} = \sum_{\psi \in \psi_m} P_{M_{k,l}} G_\psi R_\psi^{-\alpha} + \sum_{\psi \in \psi_f} P_F G_\psi R_\psi^{-\alpha} \tag{3}$$

From (3), I_M and I_{FM} denote the interference from neighbouring macrocells and femtocells respectively, while ψ represents the set of interfering base stations, with ψ_m being the set of interfering macrocells and ψ_f the set of interfering femtocells respectively. The contents of ψ_m and ψ_f depend on the location and type of UE being interfered. As earlier stated, since all sectors are symmetrical, we consider a reference UE located in sector S_{03} of M_o and define the

sets as given in **Table 1**, which are crucial in the analytical framework to be developed. Due consideration is given for all possible UE locations in the simulation.

Table 1. Notable sets of macrocells for interference analysis to sector S_{03} of cell M_0

Set	Cell ID's	Description of Set
C_a	{0 -18}	Set of all macrocells in the system
C_o	{1-18}	All macrocells that use sub-band A (CCR spectrum) and will interfere with a UE in CCR of cell M_o
C_1	{5, 14, 15, 16}	Macrocells on sub-band B causing interference in S_{03} of M_o
C_2	{NIL}	Macrocells that use sub-band C and will cause interference in S_{03} of M_o
C_3	{3, 10, 11}	Macrocells on sub-band D causing interference in S_{03} of M_o
C_4	{2, 9}	Macrocells that use sub-band E and will cause interference in S_{03} of M_o
C_5	{1, 7, 8}	Macrocells on sub-band F and will cause interference in S_{03} of M_o
C_6	{NIL}	Macrocells that use sub-band G and will cause interference in S_{03} of M_o

The set of femtocells that will cause interference to a UE (whether macro or femto) in any region will be those femtocells that share same spectrum with the specified UE in any region. Because the femtocells are distributed according to a spatial PPP, the set of interfering femtocells can only be approximated as a marked Spatial PPP which is a subset of the total femtocell set Ω_f, since the independent thinning of a PPP leads to another PPP [17], thereby conserving the irregular structure of the femtocell distribution. The total density of λ_f is therefore weakened either by probability of having interfering femtocell in same region with intended user, probability of accessing same sub-band as intended UE from a set of usable sub-bands in a region or both.

3. Interference Analysis and Coverage Probability

The coverage probability of an MUE or FUE x on a RB n is determined when the instantaneous SINR level exceeds a certain threshold γ, which is conditioned on the locations of the MUE/ FUE and the serving and interfering base stations. It is mathematically equivalent to the complementary cumulative distribution function (CCDF) of the SINR distribution and is given as; $CP_x = \Pr(SINR_x^{n_k} > \gamma)$. It is therefore paramount to first analyze the interference statistics of all the 4 different kinds of users which will then enable us derive analytical framework for the coverage probability in each case. Taking note of AS 7, we only present the analysis for sector S_{03} of cell M_o here, due to brevity and space limitations.

3.1 CCR MUEs in sector S_{03} of cell M_o

Co-tier macro interference will emanate from all macrocells using sub-band A. $\psi_m = C_o$

Cross-tier femto interference will arise from a set of femtocells that share resources from same sub-band with center region MUEs (i.e. use sub-band A), and these are only a portion of the edge region femtocells. Hence, this set of interfering femtocells would be a thinned version of the initial SPPP which may be represented as $\Omega_{f_{E-C}}$ with intensity $q_{mc}\lambda_f$, where $0 < q_{mc} < 1$ (such that $q_{mc}\lambda_f < \lambda_f$), is a function of:

- the interfering femtocells being located in the edge area with probability, p_{f-edge}

- the interfering femtocells use sub-band A in the edge area

Therefore, the set of interfering femtocells to CCR MUES is $\psi_f = \bigcup_{k \in C_a} \Omega^k_{f_{E-C}}$ and we can have;

$$I_M = \sum_{\psi \in C_0} P_m G_\psi R_\psi^{-\alpha} \text{ and } I_{FM} = \sum_{\kappa \in C_a} \sum_{\psi \in \Omega^k_{f_{E-C}}} P_f \vartheta G_\psi R_\psi^{-\alpha} \tag{4}$$

Lemma 1: Considering the location of an MUE in CCR, its coverage probability can thus be expressed as in (5) when averaged over the center region;

$$CP_{mc} = \frac{2}{R_m^{\,2} - R_0^{\,2}} \int_{R_0}^{R_m} \exp\left(-\frac{\mu\gamma r^\alpha \sigma^2}{P_{M_{0l}}} \right) \left(\sum_{i \in \psi_m} \frac{1}{1 + \gamma \left(\frac{r}{\|r - b_i\|} \right)^\alpha} \right) \times \exp\left(-\pi q_{mc} \lambda_f . \left(\mu\gamma r^\alpha \vartheta \frac{P_f}{P_m} \right)^{\frac{2}{\alpha}} \Gamma\left(1 - \frac{2}{\alpha}\right) \Gamma\left(\frac{2+\alpha}{\alpha}\right) \right) . r \, \mathrm{dr} \tag{5}$$

Proof: From the definition above, the coverage probability of a UE in center region is given as;

$$(CP_{mc} \mid r, \theta) = \mathrm{E}_{r,\theta}\left[\mathrm{P}(SINR > \gamma \mid \mathrm{r}, \theta) \right] = \oint_{S_{CR}} \mathrm{P}\left(SINR > \gamma \mid \mathrm{r}, \theta \right) \mathrm{ds} \tag{6}$$

With uniform UE distribution in the CCR, and since UEs are defined by distance and angle in polar coordinates, the coverage probability averaged over the center area is expressed as;

$$\left(CP_{mc} \mid r, \theta \right) = \int_0^{2\pi} \int_{R_L}^{R_H} \mathrm{P}\left(SINR > \gamma \mid \mathrm{r}, \theta \right) . f_r(\mathrm{r}) \, f_\theta(\theta) \, \mathrm{dr} \, \mathrm{d}\theta \tag{7}$$

Where R_H and R_L are the upper and lower radii of the circumference defining the region where the reference UE is located (the center region in this case), $f_r(r)$ and $f_\theta(\theta)$ are the probability density function (PDF) of the user location defined by distance, r, and angular position, θ, respectively; and given as;

$$f_{r,mue}(r) = \begin{cases} \dfrac{2r}{R_m^2 - R_o^2}, & R_0 \le r \le R_m \quad \text{(CCR)} \\ \dfrac{2r}{R_C^2 - R_m^2}, & R_m \le r \le R_C \quad \text{(CER)} \end{cases} \tag{8}$$

$$f_{\theta,mue}(r) = \begin{cases} \dfrac{1}{2\pi}, & 0 \le \theta \le 2\pi \quad \text{(CCR)} \\ \dfrac{1}{\pi/3}, & \theta_L \le \theta \le \theta_H \quad \text{(CER)} \end{cases} \tag{9}$$

R_0 is the minimum distance of a UE from serving base station (25m in this work), R_m and R_C are as earlier defined, θ_L and θ_H are the lower and upper angle limits of the region surrounding the considered UE ($\pi/6$ and $\pi/2$ respectively for the sector S_{03} of cell M_o in consideration). Since the CCR utilizes an omnidirectional antenna, the interference performance for CCR MUEs will have isotropic performance and the instantaneous SINR will vary very little with polar angle as shown in [31]. Hence, the coverage probability $CP_{mc} \mid r, \theta$ can be re-written as $CP_{mc} \mid r$, and expressed as;

$$CP_{mc} = \frac{2}{R_m^2 - R_0^2} \int_{R_0}^{R_m} \mathrm{P}\left(SINR > \gamma \mid \mathrm{r} \right) r \, \mathrm{dr} \tag{10}$$

After simplifying the integral term, and considering Rayleigh fading, $g_m = \exp(\mu)$;

$$\mathrm{P}[SINR > \gamma] = \mathrm{E}_{I_M, I_{FM}}\left[\mathrm{P}\left[-\mu\left(\sigma^2 + I_M + I_{FM}\right)\frac{\gamma r^{\alpha}}{P_m}\right]\right] \tag{11}$$

This simplifies to;

$$\mathrm{P}[SINR > \gamma] = e^{-\frac{\mu\gamma r^{\alpha}\sigma^2}{P_m}}.\mathrm{E}_{I_M}\left[e^{-\frac{\mu\gamma r^{\alpha}}{P_m}I_M}\right].\mathrm{E}_{I_{FM}}\left[e^{-\frac{\mu\gamma r^{\alpha}}{P_m}I_{FM}}\right] = e^{-\frac{\mu\gamma r^{\alpha}\sigma^2}{P_m}}.\mathcal{L}_{I_M}\left(\frac{\mu\gamma r^{\alpha}}{P_m}\right).\mathcal{L}_{I_{FM}}\left(\frac{\mu\gamma r^{\alpha}}{P_m}\right) \tag{12}$$

Where $\mathcal{L}_{I_M}(s)$ and $\mathcal{L}_{I_{FM}}(s)$ represent the Laplace transforms of the random variables I_M and I_{FM} respectively, evaluated at $s\left(s = \frac{\mu\gamma r^{\alpha}}{P_m}\right)$.Substituting (12) into (10);

$$CP_{mc} = \frac{2}{R_m^2 - R_0^2}\int_{R_L}^{R_H} e^{-\frac{\mu\gamma r^{\alpha}\sigma^2}{P_m}}.\mathcal{L}_{I_M}\left(\frac{\mu\gamma r^{\alpha}}{P_m}\right).\mathcal{L}_{I_{FM}}\left(\frac{\mu\gamma r^{\alpha}}{P_m}\right)r\,\mathrm{dr} \tag{13}$$

From (4), I_M is a weighted sum of independent exponential random variables, and hence $\mathcal{L}_{I_M}$ can be represented by the moment generating function (MGF) of exponential distribution [32].

$$\mathcal{L}_{I_M} = \mathrm{M}_{I_{FM}} = \sum_{i\in\Psi_m}\frac{\mu}{\mu + \frac{\mu\gamma r^{\alpha}}{P_m}.P_i R_i^{-\alpha}} = \sum_{i\in\Psi_m}\frac{1}{1+\gamma\left(\frac{r}{\|r-b_i\|}\right)^{\alpha}} \tag{14}$$

Since P_m=P_i=P for all macro base stations, and $R_i = r - b_i$, where r is the distance vector from the center cell M_0 to the UE under consideration and b_i represents the distance vector from M_0 to the interfering macrocell M_i. The femto interference I_{FM} follows a Poissonian-shot noise process [30], and the evaluation of its Laplace transform is given below;

$$\mathcal{L}_{I_{FM}}(s) = E_{G_i,\Psi_f}\left[\exp -s\left(\sum_{i\in\Psi_f}P_F\vartheta G_i R_i^{-\alpha}\right)\right] = \mathrm{E}_{\Psi_f}\left(\prod_{i\in\Psi_f}\mathcal{L}_g\left(sR_i^{-\alpha}\vartheta P_f\right)\right) \tag{15}$$

By slight change of notation and from probability generating functional (PGFL) of the PPP,

$$\mathcal{L}_{I_{FM}}(s) = \exp\left(-2\pi q_{me}\lambda_f\int_r^{\infty}\left(1-\mathcal{L}_g\left(sx^{-\alpha}\vartheta P_f\right)\right)x\,\mathrm{dx}\right) \tag{16}$$

By change of integration order and substituting for $\mathcal{L}_g\left(sx^{-\alpha}\vartheta P_f\right)$, we get;

$$\mathcal{L}_{I_{FM}}(s) = \exp\left(-2\pi q_{me}\lambda_f\underbrace{\int_0^{\infty}\int_r^{\infty}\left(1-e^{-sx^{-\alpha}\vartheta P_f g}\right)f(g)x\,\mathrm{dxdg}}_{(Y)}\right) \tag{17}$$

After integration by parts and using the Gamma function properties;

$$Y = \frac{1}{2}\left(s\vartheta P_f\right)^{\frac{2}{\alpha}}\Gamma\left(1-\frac{2}{\alpha}\right)\mathrm{E}_g\left(g^{\frac{2}{\alpha}}\right) \tag{18}$$

Substituting for Y and using the relation $\mathrm{E}_g\left(g^{\frac{2}{\alpha}}\right) = \Gamma\left(\frac{2+\alpha}{\alpha}\right)$, for $\alpha > 2$;

$$\mathcal{L}_{I_{FM}}(s) = \exp\left(-\pi q_{me}\lambda_f.\left(\mu\gamma r^{\alpha}\vartheta\frac{P_f}{P_m}\right)^{\frac{2}{\alpha}}\Gamma\left(1-\frac{2}{\alpha}\right)\Gamma\left(\frac{2+\alpha}{\alpha}\right)\right) \tag{19}$$

Substituting $\mathcal{L}_{I_M}(s)$ and $\mathcal{L}_{I_{FM}}(s)$ in (13) gives the result. ■

3.2 CER MUEs in sector S_{03} of cell M_0

Co-tier macro interference will emanate from all macrocells using sub-band B and radiating towards S_{03} of cell M_o. $\psi_m = C_1$

Cross-tier femto interference will arise from a set of femtocells using sub-band B to serve attached FUEs and this represents all femtocells in sectors S_1, S_5 and S_6 with thinned density, $q_{me}\lambda_f$, where $0 < q_{me} < 1$ (such that $q_{me}\lambda_f < \lambda_f$) is a function of the interfering femtocells belonging to sectors S_1, S_5 and/or S_6 with probability $p_{f-S_1 \cup S_5 \cup S_6}$, represented by the PPP $\Omega_{S_1 U S_5 U S_6}$.

Hence the set of interfering femtocells for CER MUEs is $\psi_f = \bigcup_{k\in\{\mathrm{B}\}} \Omega^k{}_{S_1 U S_5 U S_6 \in C_a}$

Lemma 2: The coverage probability of a CER MUE averaged over sector S_{03} of M_0 is approximated as in (20).

$$CP_{me} = \frac{1}{\pi/3}\cdot\frac{2}{R_C{}^2 - R_m{}^2}\int_{R_m}^{R_C}\int_{\pi/6}^{\pi/2}\exp\left(-\frac{\mu\gamma r^{\alpha}\sigma^2}{P_{M_{0l}}}\right)\times\left(\sum_{i\in\psi_m}\frac{1}{1+\gamma\left(\frac{r}{\|r-b_i\|}\right)^{\alpha}}\right)$$
$$\times\exp\left(-\pi q_{me}\lambda_f\cdot\left(\mu\gamma r^{\alpha}\vartheta\frac{P_f}{P_m}\right)^{\frac{2}{\alpha}}\Gamma\left(1-\frac{2}{\alpha}\right)\Gamma\left(\frac{2+\alpha}{\alpha}\right)\right).r\,\mathrm{d}r\,\mathrm{d}\theta \quad (20)$$

The proof is similar to Lemma 1, except for a change in the PDF of user location in CER, which includes angular position in sector S_{03} of M_0, and the use of appropriate interfering macro and femto cells respectively.

3.3 CCR FUEs in sector S_{03} of cell M_0

Cross-tier macro interference will be as a result of macrocells that use sub-bands D, E, F and radiate transmissions towards sector S_{03} of cell M_o. $\psi_{m-S_3} = C_3 \cup C_4 \cup C_5$

Co-tier femto interference will emanate from a set of femtocells that use sub-band D, E and/or F, with thinned density, $q_{fc}\lambda_f$, where $q_{fc} < 1$ (such that $q_{fc}\lambda < \lambda_f$) is dependent on the interfering femtocells using sub-bands D, E and/or F with probability, $p_{f-S_1 \cup S_2 \cup S_3 \cup S_4 \cup S_5}$, implying that all femtocells in sectors S_1, S_2, S_3, S_4, and S_5 will interfere.

Lemma 3: The coverage probability of center FUEs in S_{03} of M_0 is given in (21), where r_{fue} is the distance vector from an FUE to its serving HeNB, R_{HeNB} is the radius of the serving HeNB, r is the distance vector of the tagged HeNB (and not the FUE) to macrocell M_o as stated in assumption 8.

Proof: In the case of FUEs, the PDF of FUE location in its femtocell is considered, as well as the PDF of the serving femtocell location in the respective macrocell. In addition, since the FUEs in consideration are in sector S_{03} of M_0, the expectation over the angular position is also considered. The rest of the proof is same as Lemma 1. Double-wall penetration loss ϑ^2 is hereby used since the interference signal from one femtocell to another goes through double walls for both buildings.

$$CP_{fc} = \frac{1}{\pi/3}.\frac{2}{R_{HeNB}{}^2}\frac{2}{R_f{}^2}\int_0^{R_{HeNB}}\int_0^{R_f}\int_{\pi/6}^{\pi/2}\exp\left(-\frac{\mu\gamma r_{fue}{}^{\alpha}\sigma^2}{P_f}\right)\times\left(\sum_{i\in\Psi_m}\frac{1}{1+\gamma\vartheta\frac{P_m}{P_f}\left(\frac{r_{fue}}{\|r-b_i\|}\right)^{\alpha}}\right)\times \exp\left(-\pi q_{fc}\lambda_f.\left(\mu\gamma r_{fue}{}^{\alpha}\vartheta^2\right)^{\frac{2}{\alpha}}\Gamma\left(1-\frac{2}{\alpha}\right)\Gamma\left(\frac{2+\alpha}{\alpha}\right)\right).r_{fue}r\,\mathrm{dr}_{\mathrm{HeNB}}\mathrm{drd}\,\theta \quad (21)$$

3.4 CER FUEs in sector S_{03} of cell M_0

If FUE is in CER, it can either use sub-band A, or the 3 the edge sub-bands - D, E and F. Cross-tier macro interference will either be as a result of macrocells that use sub-bands A or those that use sub-bands D, E and/or F radiating transmissions towards sector S_{03} of cell M_o.

$$\Psi_m = \left(\frac{\mathcal{F}_C}{\mathcal{F}_{(A+D+E+F)}} * \Psi_{C_a}\right) + \left(\frac{\mathcal{F}_{(D+E+F)}}{\mathcal{F}_{(A+D+E+F)}} * \Psi_{m-S_3}\right) \quad (22)$$

Where $\mathcal{F}_C$ denotes the number of resource blocks in the center region, and $\mathcal{F}_{\mathcal{S}_i}$ denotes the number of resource blocks in set $\mathcal{S}_i$, which contains elements as listed respectively.

For co-tier femto interference, if the reference FUE uses sub-band A, all edge femtocells using sub-band A will interfere, while if its uses D, E and/or F, all femtocells in the entire macrocell area using D, E, F will interfere.

$$\lambda_{FF-S_3} = \left(\frac{\mathcal{F}_C}{\mathcal{F}_{(A+D+E+F)}} * q_{mc}\lambda_f\right) + \left(\frac{\mathcal{F}_{(D+E+F)}}{\mathcal{F}_{(A+D+E+F)}} * q_{fc}\lambda_f\right) \quad (23)$$

Where $\lambda_{FF-S_3} < \lambda_f$

Lemma 4: The coverage probability for a CER MUE averaged over sector S_{03} of M_0 is given in (24). The proof is same as Lemma 3, with only a change in the respective interfering macro and femtocells.

$$CP_{fe} = \frac{1}{\pi/3}.\frac{2}{R_{HeNB}{}^2}\frac{2}{R_c{}^2 - R_f{}^2}\int_0^{R_{HeNB}}\int_{R_f}^{R_c}\int_{\pi/6}^{\pi/2}\exp\left(-\frac{\mu\gamma r_{fue}{}^{\alpha}\sigma^2}{P_f}\right)\times\left(\sum_{i\in\Psi_m}\frac{1}{1+\gamma\vartheta\frac{P_m}{P_f}\left(\frac{r_{fue}}{\|r-b_i\|}\right)^{\alpha}}\right)\times \exp\left(-\pi\lambda_{FF-S_3}.\left(\mu\gamma r_{fue}{}^{\alpha}\vartheta^2\right)^{\frac{2}{\alpha}}\Gamma\left(1-\frac{2}{\alpha}\right)\Gamma\left(\frac{2+\alpha}{\alpha}\right)\right).r_{fue}r\,\mathrm{dr}_{\mathrm{HeNB}}\mathrm{drd}\,\theta \quad (24)$$

It is to be noted that the effects of antenna azimuth for sector antennas were found to be insensitive to user SINR distribution in [19] and hence have not been considered in this work for space limitations and better tractability.

4. Performance Metrics and Optimal Design

4.1 Throughput

Having derived the SINR distribution for the different kinds of UEs, the average network throughput can thus be derived under the proposed resource allocation scheme in the following section. It is assumed that each user (both MUEs and FUEs) provides feedback of its

instantaneous downlink SINR on every assigned resource block to the serving base station, with which the base station determines the transmission rate using an adaptive modulation and coding (AMC) scheme with L discrete levels [4]. Let b_l (bps/Hz) represent the instantaneous transmission rate of a sub-channel assuming its instantaneous SINR lies in $[\gamma_l, \gamma_{l+1})$, $1 \le l \le L$.

Hence, $$b_l = \log_2(1+\frac{\gamma_l}{\Phi}) \text{ bps/Hz} \tag{25}$$

When $SIR \in [\gamma_l, \gamma_{l+1}),\ 1 \le l \le L$

where Φ is the Shannon gap reflecting variation between Shannon capacity and practical transmission according to AMC [7]. As a result, the long-term expected throughput (in bps/Hz) in each sub-channel is given as;

$$t = \sum_{l=1}^{L-1} b_l . \Pr\left[\gamma_l \le SIR < \gamma_{l+1}\right] + b_L . \Pr\left[SIR \ge \gamma_L\right] \tag{26}$$

Using the coverage probability results derived in section 3, we can express the above formulation as;

$$t_j = \sum_{l=1}^{L-1} b_l . \left(\mathrm{P}_{C_j}(\gamma_l) - \mathrm{P}_{C_j}(\gamma_{l+1})\right) + b_L . \mathrm{P}_{C_j}(\gamma_L) \tag{27}$$

where the subscript j could represent the CCR MUE, CER MUE, CCR FUE or CER FUE as the case maybe and P_c denotes the coverage probability. For simplification, we can assume $b_l = l$ and $\gamma_l = \Phi(2^l - 1)$, for $l = 1, ...L$. Hence,

$$t_j = \sum_{l=1}^{L-1} l . \left(\mathrm{P}_{C_j}(\gamma_l) - \mathrm{P}_{C_j}(\gamma_{l+1})\right) + b_L . \mathrm{P}_{C_j}(\gamma_L) \tag{28}$$

The expected throughput in each macrocell/femtocell is thereby obtained by the product of (28) with the respective spectrum allocation factor. The spectrum allocation factor for the center region is defined as $\rho = |\mathcal{F}_C| / |\mathcal{F}_T|$, where $\mathcal{F}_C$ is as earlier defined and $\mathcal{F}_T$ denotes the total resource blocks available in the system. Therefore, the expected throughput for all the different kinds of UEs will be given as;

$$\begin{cases} T_{M_{CR}} = \rho . t_{M_{CR}} \\ T_{M_{ER}} = (1-\rho) . t_{M_{ER}} \\ T_{F_{CR}} = (1-\rho)/2 . t_{F_{CR}} \\ T_{F_{ER}} = \left(\rho + (1-\rho)/2\right) . t_{F_{ER}} \end{cases} \tag{29}$$

In total, the macrocell network throughput in cell M_0 is therefore expressed as;

$$T_{\text{macro.}} = \rho t_{M_{CR}} + (1-\rho) t_{M_{ER}} \tag{30}$$

While the femtocell network throughput is;

$$T_{femto} = \frac{1}{2}(1-\rho) . t_{F_{CR}} N_{F_{CR}} + \left(\frac{\rho+1}{2}\right) . t_{F_{ER}} N_{F_{ER}} \tag{31}$$

Where $N_{F_{CR}} = \lambda_f . \pi R_f^{\ 2}$ and $N_{F_{ER}} = \lambda_f . \pi \left(R_C^{\ 2} - R_f^{\ 2}\right)$ represent the average number of femtocells in the CCR and CER respectively.

4.2 Harmonic Mean

Usually mobile networks aim to maximize total spectral efficiency, but this may often be realized at the cost of unfair allocation of resources to UEs at the cell-edge. In FFR networks, the asymmetric spatial partitioning of the coverage area has a significant influence on resource allocation to the various cell regions. Depending on the resource allocation scheme and

especially for non-uniform UE distribution, this could lead to poor user throughput for certain edge UEs even while the total network throughput could be at the maximum. It was shown in [12] how the total network spectral efficiency showed very high value due to relatively high capacity values from only three center UEs, while 21 other edge UEs had very low capacity values. This is due to the throughput for center region UEs having an outweighing dominance on the total macro throughput with increasing spectrum allocation factor to the center, thereby skewing the total network throughput in favor of center region UEs always as evident from (30). Hence, to improve on this fairness for all UEs irrespective of location, the harmonic mean metric is hereby proposed. The harmonic concept in resource allocation was initially introduced in [14] for determining appropriate time-resource ratio and spatial partitioning criterion for cell regions. The harmonic mean, *H*, is generally more stable for outliers and is often seen to be the most accurate of means. Mathematically, it is defined as the reciprocal of the arithmetic mean of reciprocals. From the definition, let Z_m and Z_f represent the mean of reciprocals for macro throughput and femto throughput respectively,

$$Z_m = \frac{1}{\frac{\frac{1}{\rho t_{M_{CR}}} + \frac{1}{(1-\rho)t_{M_{ER}}}}{2}} = \frac{1}{\frac{1}{2}\left(\frac{(1-\rho)t_{M_{ER}} + \rho t_{M_{CR}}}{\rho t_{M_{CR}}(1-\rho)t_{M_{ER}}}\right)} \text{ and } Z_f = \frac{1}{\frac{\frac{1}{\frac{1}{2}(1-\rho).t_{F_{CR}}N_{F_{CR}}} + \frac{1}{\left(\frac{\rho+1}{2}\right).t_{F_{ER}}N_{F_{ER}}}}{2}} \tag{32}$$

Harmonic mean is the inverse of the mean of reciprocals. Hence,

$$H_{macro} = \frac{1}{Z_m} = \frac{2\rho t_{M_{CR}}(1-\rho)t_{M_{ER}}}{(1-\rho)t_{M_{ER}} + \rho t_{M_{CR}}} \tag{33}$$

$$H_{femto} = \frac{1}{Z_f} = \frac{(1-\rho)N_{F_{CR}}t_{F_{CR}}(\rho+1)N_{F_{ER}}t_{F_{ER}}}{(\rho+1)N_{F_{ER}}t_{F_{ER}} + (1-\rho)N_{F_{CR}}t_{F_{CR}}} \tag{34}$$

4.3 Optimal Network Design

From the analytical expressions derived, it is obvious that the appropriate choice of key FFR-related parameters is expected to have a significant effect on the network performance. In this section, we intend to derive some of these optimal parameters for the two-tier network (the spatial partitioning threshold, $\omega = R_m/R_C$, and the spectrum allocation factor, $\rho = |\mathcal{F}_C|/|\mathcal{F}_T|$) which maximize the average network throughput while ensuring fairness in resource allocation among the UEs in different regions through the harmonic mean metric. Using the area-proportional design, where the resources allocated to each region is proportional to the area of that region, more equitable distribution of resources is guaranteed to both center and edge regions. Based on such approach,

$$\frac{\pi R_m^{\,2}}{\left(\pi R_C^{\,2} - \pi R_m^{\,2}\right)} = \frac{\rho}{(1-\rho)} \tag{35}$$

Thus, $\rho = \omega^2$ (or $\omega = \sqrt{\rho}$). The net average macro throughput per sub-channel will therefore depend on the optimization factors ρ and ω as given in (36);

$$T_{\text{macro.}}(\rho,\omega) = \rho t_{M_{CR}}(\rho,\omega) + (1-\rho)t_{M_{ER}}(\rho,\omega) \tag{36}$$

The optimization problem based on such area-proportional design is expressed as;

$$(\rho^*,\omega^*) = \arg \max_{(0\le\rho,\omega\le 1)} \rho t_{M_{CR}}(\omega) + (1-\rho)\,t_{M_{ER}}(\omega) \tag{37}$$

Subject to $\rho = \omega^2$

Upon substituting for ρ, whose value lies within the set $\mathcal{S}_\rho$, we have;

$$\rho^* = \arg \max_{\rho \in \mathcal{S}_\rho} \rho t_{M_{CR}}(\rho, \sqrt{\rho}) + (1-\rho) t_{M_{ER}}(\rho, \sqrt{\rho}) \tag{38}$$

where $\omega^* = \sqrt{\rho^*}$

To provide more insight into the trade-offs between throughput and fairness, the spatial and spectrum threshold factors are again optimized with respect to harmonic mean. The results are compared with those from (38) and presented in section 5. Considering (36), it must be stated that for the higher, multi-user diversity scheduling procedures (the maximum SINR scheduling scheme) [31], almost all the available resources would easily be allocated to center region due to better channel conditions, leading to degraded performance for lower percentile UEs. Thus, the intent is to find ρ^* and R_m^* such that the harmonic mean is maximized as given in (39);

$$\rho^* = \arg\max_{\rho} \frac{2\rho t_{M_{CR}} (1-\rho) t_{M_{ER}}}{(1-\rho) t_{M_{ER}} + \rho t_{M_{CR}}} \text{ or } R_m^* = \arg\max_{R_m} \frac{2\rho t_{M_{CR}} (1-\rho) t_{M_{ER}}}{(1-\rho) t_{M_{ER}} + \rho t_{M_{CR}}} \tag{39}$$

s.t $\rho = \omega^2$

Furthermore, a critical analytical expression is also derived in this section for the maximum co-channel femtocells' density that can co-exist with the overlaid FFR macrocells in any region, to guarantee some given quality of service (QoS). This analytical expression provides insights into the relation of key network parameters (such as path-loss exponent, outage constraints, minimum distance of femtocell to overlaying macrocell etc.) with the femtocell density, and is especially important when provisioning heterogeneous networks with dense femtocell deployments. Assuming there is a QoS constraint for macro users such that, $\left(\Pr\left(SINR_m \le \gamma\right)\right) \le \varepsilon_m$, where $0 \le \varepsilon_m \le 1$ denotes the maximum outage constraint to guarantee successful transmission, then in order to avoid violating the outage constraint, the probability of coverage derived in (5), (20), (21) and (24) must satisfy the outage constraint in (40) [33].

$$\left(\Pr\left(SINR_m \ge \gamma\right)\right) = 1 - \varepsilon_m . \tag{40}$$

Hence, for an interference limited scenario (noise is zero), and focusing only on effect of femto-interference, (5) is re-written as;

$$\frac{2}{R_C^{\,2} - R_m^{\,2}} \int_{R_m}^{R_C} \exp\left(\frac{-\pi q_{mc} \lambda_f \cdot \left(\mu \gamma r^\alpha \vartheta \frac{P_f}{P_m} \right)^{\frac{2}{\alpha}}}{\Gamma\left(1 - \frac{2}{\alpha}\right) \Gamma\left(\frac{2+\alpha}{\alpha}\right)} \right) r . \mathrm{d}r = 1 - \varepsilon_m \tag{41}$$

Re-arranging and using the relation (42) from [34], we derive the important expression in (43).

$$\Gamma\left(1 - \frac{2}{\alpha}\right) \Gamma\left(\frac{2+\alpha}{\alpha}\right) = \frac{2\pi}{\alpha \sin\left(\frac{2\pi}{\alpha}\right)} \tag{42}$$

The expression in (43) provides the maximum co-channel femtocell density that can be deployed in the center region in co-existence to center region MUEs, without violating the outage constraint ε_m of a CCR MUE located at position $R_0 \le r \le R_m$. It is interesting to see how this easily shows the relation of the maximum co-channel femtocell density for a given MUE with different network parameters, particularly its inverse relation with the distance of the considered MUE from its serving MeNB, r for a defined set of outage constraints (ε_m and γ).

$$\left(q_{mc}\lambda_f\right)^* = -\frac{\ln\left(\frac{1-\varepsilon_m\left(R_m^{\,2}-R_0^{\,2}\right)}{2}\right)\alpha\sin\left(\frac{2\pi}{\alpha}\right)}{2\pi^2\int_{R_m}^{R_C}\left(\mu\gamma r^{\alpha}\vartheta\frac{P_f}{P_m}\right)^{\frac{2}{\alpha}} r\,\mathrm{d}r} \tag{43}$$

The relation in (43) is also a function of the path-loss exponent α, the radii of the region housing the UE, and importantly, the signal-to-interference ratio of the macrocell to femtocell given P_m/P_f. Femtocells could employ some power-control to control interference to the MUEs for managing the outage constraint. Similar procedure can be used for the other UEs – (CER MUEs, CCR FUEs, and CER FUEs) to derive the maximum allowable co-channel femtocell density for successful transmission.

5. Analytical and Simulation Results

This section validates the proposed analytical framework and provides some system design guidelines for such multi-tier OFDMA networks. Numerical results obtained are from about 10,000 Monte Carlo simulations. The cellular network is composed of 19 macrocells with hexagon tessellation, where the reference cell is at the center surrounded by two layers of interfering macrocells, and the femtocells distributed according to a spatial PPP as earlier stated, with intensity λ_f. The main system parameters used are given in **Table 2** for the downlink of a typical LTE/LTE-A network.

Table 2. Simulation Parameters

Parameters	**Values**		
	Macro		Femto
Topology	6-sectored, 19 Cells		PPP. $\lambda_f = 0.00005 \sim 0.001$ FBS/m^2
Coverage Radius	R_{HEX} =330m		R_{HeNB} =20m
Transmit Power	43 dBm		13 dBm
No. of UEs	50 per MeNB		2 per HeNB
Parameters	**Values**	**Parameters**	**Values**
Carrier Frequency	2 GHz	System Bandwidth	20 MHz
No. of Resource Blocks	100	sub-carrier spacing Δf	15 KHz
Outdoor path-loss exponent	4	Indoor path-loss exponent	3
Rayleigh parameter μ	1	Shannon gap Φ	3dB
Wall-partition loss ϑ	5~15 dB	Min. distance between MeNB and UE R_0	25m
Noise Density N_0	-174 dBm/Hz	No. of adaptive modulation Levels L	8

The plots for CDF of SINR (outage probability) for all the UEs are plotted in **Fig. 3** and **Fig. 4** for different femtocell densities, where it is observed that results from the derived analytical expressions are very much in conformity with those obtained from Monte Carlo simulations. This validates the analytical framework derived for the UE SINR distribution in this work. In all cases, it is evident that with increasing femtocell deployment operating in CSG mode, the coverage performance for all UEs gets degraded which can be easily noted by the expressions

in (5), (20), (21) and (24) where the coverage is a monotonically decreasing function of λ_f.

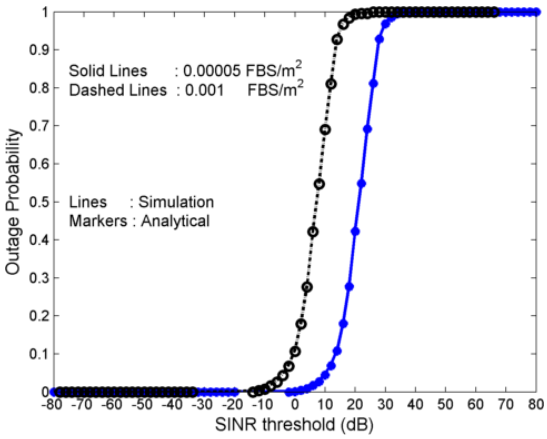

Fig. 3(a). CCR MUE Outage Probability

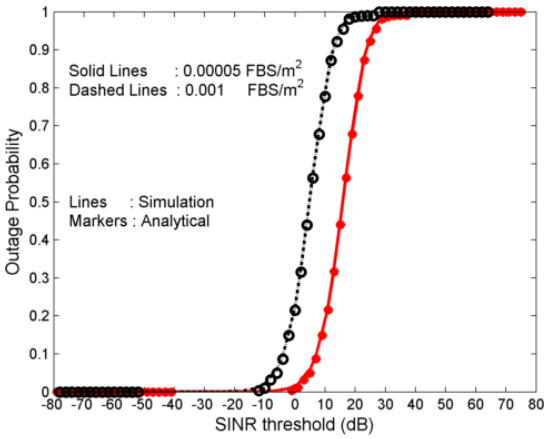

Fig. 3(b). CER MUE Outage Probability

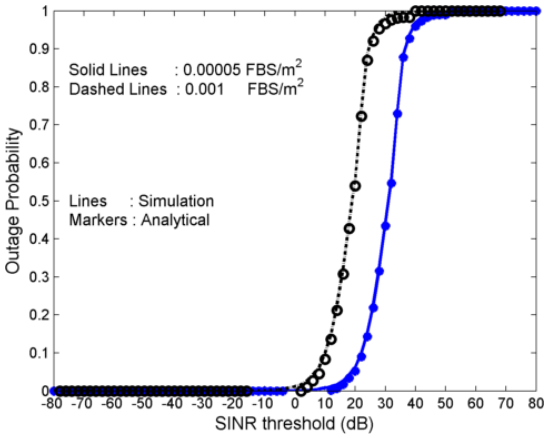

Fig. 4(a). CCR FUE Outage Probability

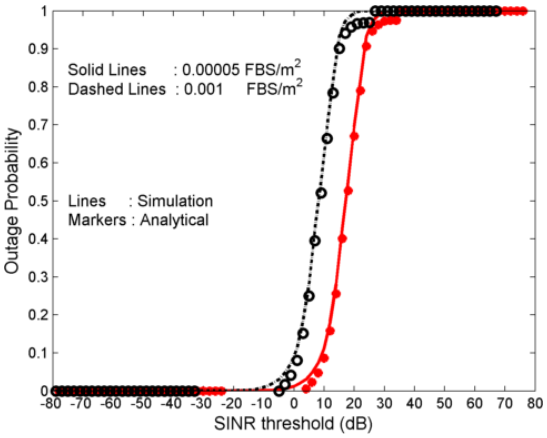

Fig. 4(b). CER FUE Outage Probability

Fig. 5 shows the relation between average macro capacity and the center region distance threshold R_m, using $T_{M_{CR}}$, $T_{M_{ER}}$ and T_{Macro} in (29) and (30) based on the area-proportional design where $\rho = \omega^2$. It can be seen how total average macro capacity is greatly influenced by the center region capacity, with the optimal ω very close to 1, resembling full spectrum usage. The average macro throughput is seen to increase with increasing MUE density in **Fig. 6** due to the increase in resource utilization as more UEs are present in both CCR and CER, thereby avoiding wastage of resources, but optimal ω is not very sensitive to increase in MUEs when using the channel-blind RR scheduler with no multi-user diversity. As expected, the reverse is the case for increasing femtocell density since there is an increase in cross-tier interference leading to performance degradation for the macro tier throughput. An interesting observation is that the optimal ω realized from **Fig. 5** is rather insensitive to increasing MUE density since the area proportional scheme distributes resources according to ratio of the respective areas and assuming uniform distribution, an increase in MUE density would be uniformly distributed over both regions. However, with increasing femtocell density per cell, the value of the optimal ω increases to favor more resource distribution to CCR UEs since higher femto-tier interference would affect ER MUEs more severely, and the scheme intending to

maximize total throughput decides to maximize CCR MUEs for maximum spectral efficiency.

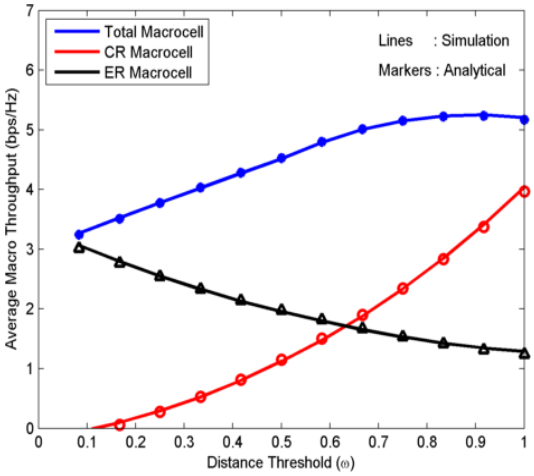

Fig. 5. Avg. macro throughput vs. distance threshold ratio (ω) when $\rho = \omega^2$

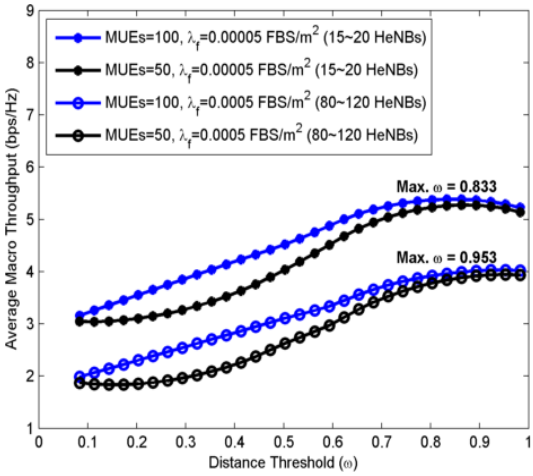

Fig. 6. Avg. Macro throughput for varying HeNB deployment and wall-partition losses.

Fig. 7 and **Fig. 8** show the second optimization method for maximizing harmonic mean scheme, in order to improve fairness between CCR and CER UEs, while ensuring femtocell performance is also not degraded at those levels. The center radius threshold R_m and the intermediary radius threshold R_f are plotted against harmonic mean of macro and femto, and the optimal values maximizing both metrics are found to be 180m (ratio of 0.6) and 235m (0.78) respectively. The implication is that at these values, the network capacity can be maximized subject to a fairness constraint to both center region and edge region, hence avoids the huge gap evident in the prior method. Looking at **Fig. 5** closely, the point at which CCR and CER average macro throughputs are equal is quite close to the optimal ω value realized from the harmonic mean method. This means the harmonic mean allows for trading some spectral efficiency for improved fairness in the system, and as seen in **Fig. 8**, the femto tier is also optimal at this point.

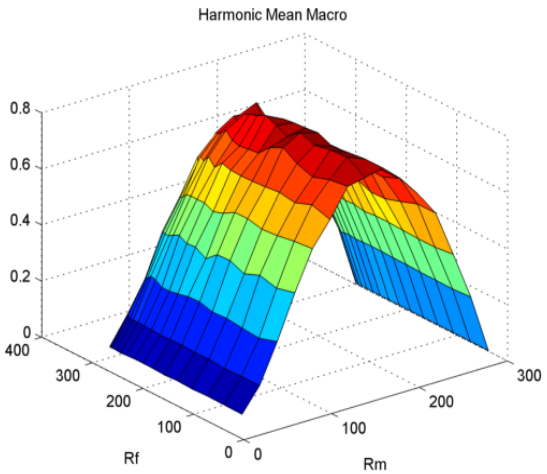

Fig. 7. Macro harmonic mean vs. the spatial partitions, R_m and R_f.

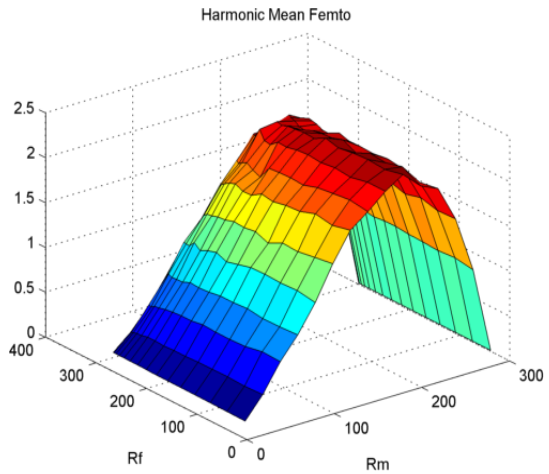

Fig. 8. Femto harmonic mean vs. the spatial partitions, R_m and R_f.

In **Fig. 9**, we compare the optimal ω values realized via maximizing both schemes, under varying femtocell deployments and wall-partition losses. The scheme maximizing average network throughput shows corresponding increase in optimal ω values with increasing femtocell density as earlier shown, while the scheme maximizing harmonic mean shows decrease in ω, albeit with less intensity. The reason here is as more femtocells are deployed, the edge region MUEs experience worse experience, and the scheme ensuring fairness adjusts to balance the resource distribution across the system. The scheme maximizing throughput shows increase in ω values with higher wall-partition losses because the femto tier interference would be absorbed higher, leading to improvements in MUE throughput especially CCR MUEs, and hence the scheme allocates more resources to the center. This is more evident for dense femtocell deployments where the femto tier interference is more severe. The fairer scheme aims to redistribute resources fairly in all cases, and hence does not show such dramatic response to femto-tier interference. It should be stated that for any scenario, the optimal spectrum allocation factor is found based on the relationship with optimal spatial threshold, $\rho = \omega^2$.

Lastly, to investigate the effect of the newly introduced intermediary region, in **Fig. 10**, the average throughput of a femtocell is compared under two different schemes using the proposed model in **Fig. 1b** and the optimal spatial thresholds realized from **Fig. 7** and **Fig. 8**. In the first scheme, the femtocell is assumed to utilize only edge spectrum bands (sub-bands B to G), while in the second scheme, the femtocell can either share same spectrum with center MUEs (sub-band A) or choose the edge spectrum bands when in the edge region, just as shown in **Fig.1b**. Initially, both schemes have same throughput because both use only edge sub-bands in center region. However, when the femtocell is located at the border of center region in second scheme, assuming it switches to using sub-band A and sharing with center MUEs, it experiences severe interference by the central macrocell. With increasing distance away from central macrocell, and considering higher resources available to center region MUEs in FFR schemes, this femtocell's throughput rises and attains similar values to the first scheme almost at the intermediary region radius (235m). From here henceforth, its throughput exceeds the scheme purely relying on edge sub-bands.

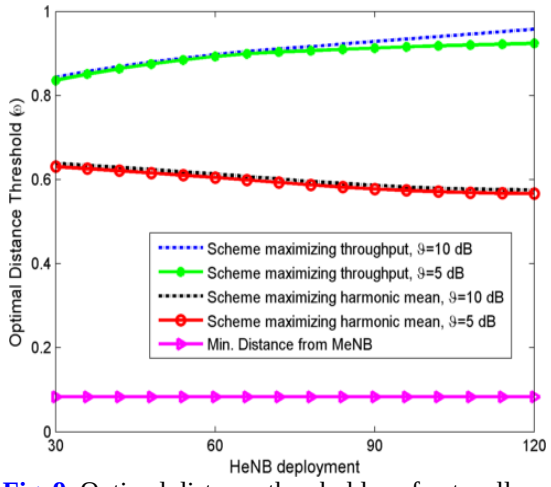

Fig. 9. Optimal distance threshold vs. femtocell deployment for both optimization methods

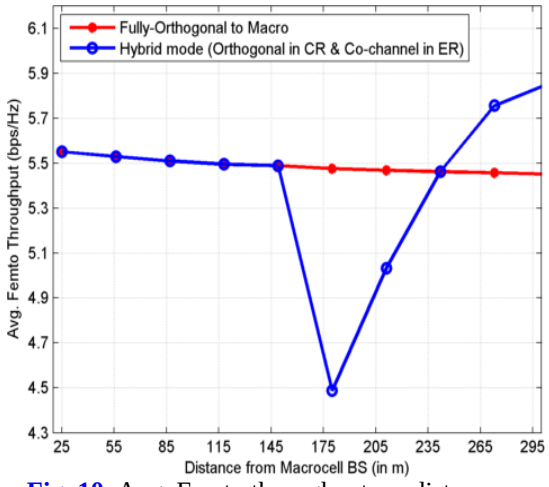

Fig. 10. Avg. Femto throughput vs. distance from central macro base station

Lastly, ten FUEs are randomly selected within the transition area of center and edge region under different schemes to analyze the interference effect. As described, when spectrum sharing is prevented between the macro and femto tiers in this zone, cross-tier interference is minimized and user SINR is improved for such UEs as shown in **Fig. 11**. The scheme employing the intermediary region offers best protection to UEs, while the full-frequency reuse scheme with no ICIC measure shows worst performance with interference arising from all access points of both tiers in all regions.

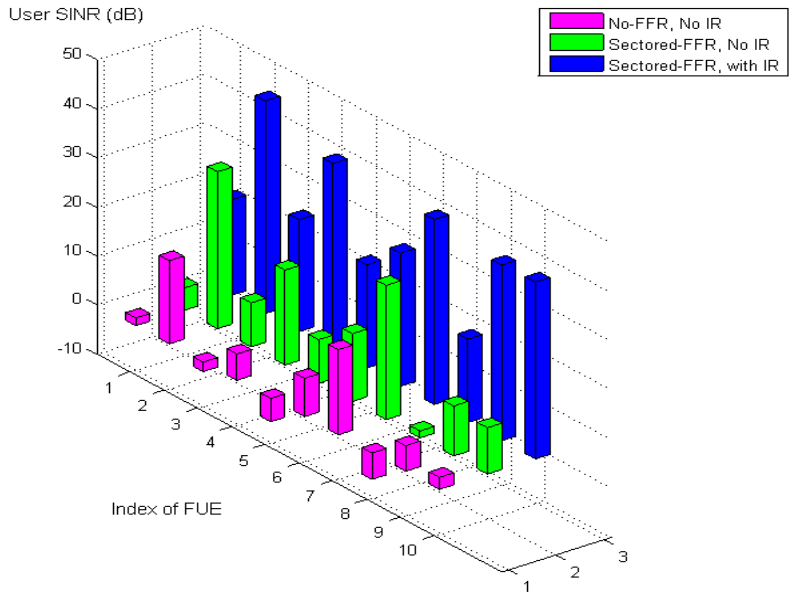

Fig. 11. SINR performance of 10 randomly selected FUEs at transition area of cell center and cell edge

6. Conclusion

In this work, an analytical framework for evaluation of two-tier FFR-aided OFDMA networks with hybrid topology of random, PPP-based femtocells and deterministic, hexagonally shaped macrocells has been provided, with a view to deriving optimal spatial and spectrum thresholds for maximizing average network throughput subject to improved fairness amongst all UEs in the system. The SINR distribution for all the different UE types is derived analytically and the results used in the analysis for average network throughput per tier and harmonic mean metric. Numerical simulations show close agreement with theoretical results, hence verifying the proposed analysis. The scheme maximizing average network throughput, yields high values of optimal spatial threshold, and consequently more resource allocation to center region, which increases further with dense femtocell deployments and higher wall-penetration losses. However, increasing number of MUEs per cell has little effect on optimal ω when the RR scheduler is used since there is no multi-user diversity to benefit from. For maximizing the harmonic mean, the optimal spatial threshold is less sensitive to femtocell density, and minimizes the gap between cell-center and cell-edge network throughput, without degrading femtocell performance.

Finally, the newly introduced intermediary region is shown to improve performance of UE at the boundary of cell center and cell-edge, and is suitable for scenarios where hybrid

spectrum usage of femtocells with overlaid macrocells is required. In such scenarios, femtocells in close proximity to central macrocells could employ orthogonal spectrum usage, while those located farther away, can employ co-channel spectrum usage for efficient spectrum utilization. As a further step to this work, the analysis will be extended to dynamic FFR schemes with varying load conditions overlaid with open-access femtocells, where some MUEs could be off-loaded to nearby small cells for better performance.

References

[1] D.-L. P. Xiaolu Chu, Yang Yang, Fredrik Gunnarasson, *Heterogeneous Cellular Networks Theory, Simulation and Deployment*. New York, United States of America: Cambridge University press, 2013. Article (CrossRef Link)

[2] J. G. Andrews, "Seven ways that HetNets are a cellular paradigm shift," *IEEE Communications Magazine*, vol. 51, no.3, pp. 136-144, 2013. Article (CrossRef Link)

[3] V. Chandrasekhar, M. Kountouris, and J. G. Andrews, "Coverage in multi-antenna two-tier networks," *IEEE Transactions on Wireless Communications*, vol. 8, no. 10, pp. 5314-5327, 2009. Article (CrossRef Link)

[4] V. Chandrasekhar and J. G. Andrews, "Spectrum allocation in tiered cellular networks," *IEEE Transactions on Communications*, vol. 57, no.10, pp. 3059-3068, 2009. Article (CrossRef Link)

[5] T. Zahir, K. Arshad, A. Nakata, and K. Moessner, "Interference management in femtocells," *IEEE Communications Surveys & Tutorials*, vol. 15, no.1, pp. 293-311, 2013. Article (CrossRef Link)

[6] T. Novlan, J. G. Andrews, S. Illsoo, R. K. Ganti, and A. Ghosh, "Comparison of fractional frequency reuse approaches in the OFDMA cellular downlink," in *Proc. of IEEE Global Telecommunications Conference* (*GLOBECOM 2010*), pp. 1-5, December 6-10, 2010. Article (CrossRef Link)

[7] J. Wha Sook, K. Juhee, and J. Dong Geun, "Downlink radio resource partitioning with fractional frequency reuse in femtocell networks," *IEEE Transactions on Vehicular Technology*, vol. 63, no.1, pp. 308-321, 2014. Article (CrossRef Link)

[8] E. Dinc and M. Koca, "On dynamic fractional frequency reuse for OFDMA cellular networks," in *Proc. of 24th IEEE International Symposium on Personal Indoor and Mobile Radio Communications* (*PIMRC*), pp. 2388-2392, September 8-11, 2013. Article (CrossRef Link)

[9] O. G. Aliu, M. Mehta, M. A. Imran, A. Karandikar, and B. Evans, "A new cellular-automata-based fractional frequency reuse scheme," *IEEE Transactions on Vehicular Technology*, vol. 64, no.4, pp. 1535-1547, 2015. Article (CrossRef Link)

[10] A. S. Mohamed, M. Abd-Elnaby, and S. A. El-Dolil, "Self-organised dynamic resource allocation scheme using enhanced fractional frequency reuse in long term evolution-advanced relay-based networks," *IET Communications*, vol. 10, no. 10, pp. 1163-1174, 2016. Article (CrossRef Link)

[11] N. Saquib, E. Hossain, and K. Dong In, "Fractional frequency reuse for interference management in LTE-advanced hetnets," *IEEE Wireless Communications*, vol.20, no.2, pp. 113-122, 2013. Article (CrossRef Link)

[12] D. Bilios, C. Bouras, V. Kokkinos, A. Papazois, and G. Tseliou, "Selecting the optimal fractional frequency reuse scheme in long term evolution networks," *Wireless personal communications*, vol. 71, no.4, pp. 2693-2712, 2013. Article (CrossRef Link)

[13] S. Kumar, S. Kalyani, and K. Giridhar, "Optimal design parameters for coverage probability in fractional frequency reuse and soft frequency reuse," *IET Communications*, vol. 9, no.10, pp. 1324-1331, 2015. Article (CrossRef Link)

[14] C.-Y. Oh, M. Y. Chung, H. Choo, and T.-J. Lee, "Resource allocation with partitioning criterion for macro-femto overlay cellular networks with fractional frequency reuse," *Wireless personal communications*, vol. 68, no.2, pp. 417-432, 2013. Article (CrossRef Link)

[15] S. U. Abdullahi, L. Jian, H. Ci, and Z. Xiaonan, "Enhancing throughput performance in LTE-Advanced Hetnets with buffered Fractional Frequency Reuse," in *Proc. of IEEE Eighth*

International Conference on Ubiquitous and Future Networks (*ICUFN*), pp. 918-923, July 5-8, 2016. Article (CrossRef Link)

[16] J. G. Andrews, F. Baccelli, and R. K. Ganti, "A tractable approach to coverage and rate in cellular networks," *IEEE Transactions on Communications*, vol. 59, no. 11, pp. 3122-3134, 2011. Article (CrossRef Link)1

[17] M. Haenggi, J. G. Andrews, F. Baccelli, O. Dousse, and M. Franceschetti, "Stochastic geometry and random graphs for the analysis and design of wireless networks," *IEEE Journal on Selected Areas in Communications*, vol. 27, no. 7, pp. 1029-1046, 2009. Article (CrossRef Link)

[18] L. Liu, T. Peng, P. Zhu, Z. Qi, and W. Wang, "Analytical evaluation of throughput and coverage for FFR in OFDMA cellular network," in *Proc. of IEEE 83rd Vehicular Technology Conference* (*VTC Spring*), pp. 1-5, May 15-18, 2016. Article (CrossRef Link)

[19] B. B, x, aszczyszyn, and M. K. Karray, "Spatial distribution of the SINR in poisson cellular networks with sector antennas," *IEEE Transactions on Wireless Communications*, vol. 15, no.1, pp. 581-593, 2016. Article (CrossRef Link)

[20] T. D. Novlan, R. K. Ganti, A. Ghosh, and J. G. Andrews, "Analytical evaluation of fractional frequency reuse for heterogeneous cellular networks," *IEEE Transactions on Communications*, vol. 60, no.7, pp. 2029-2039, 2012. Article (CrossRef Link)

[21] R. W. Heath, M. Kountouris, and T. Bai, "Modeling heterogeneous network interference using Poisson point processes," *IEEE Transactions on Signal Processing*, vol. 61, no.16, pp. 4114-4126, 2013. Article (CrossRef Link)

[22] H. ElSawy, E. Hossain, and M. Haenggi, "Stochastic geometry for modeling, analysis, and design of multi-tier and cognitive cellular wireless networks: A Survey," *IEEE Communications Surveys & Tutorials*, vol. 15, no.3, pp. 996-1019, 2013. Article (CrossRef Link)

[23] F. Wang and W. Wang, "Analytical modeling of downlink power control in two-tier femtocell networks," in *Proc. of IEEE 9th International Conference on Wireless and Mobile Computing, Networking and Communications* (*WiMob 2013*), pp. 559-564, October 7-9, 2013. Article (CrossRef Link)

[24] F. Jin, R. Zhang, and L. Hanzo, "Fractional frequency reuse aided twin-layer femtocell networks: analysis, design and optimization," *IEEE Transactions on Communications*, vol. 61, no.5, pp. 2074-2085, 2013. Article (CrossRef Link)

[25] J. García-Morales, G. Femenias, and F. Riera-Palou, "Performance analysis and optimisation of FFR-aided OFDMA networks using channel-aware scheduling," *Mobile Networks and Applications*, pp. 1-15, 2016. Article (CrossRef Link)

[26] F. Wang and W. Wang, "Analytical evaluation of femtocell deployment in cellular networks using fractional frequency reuse," *IET Communications*, vol. 8, no.9, pp. 1599-1608, 2014. Article (CrossRef Link)

[27] 3GPP TR 36.814, "Evolved Universal Terrestrial Radio Access (E-UTRA); Further advancements for E-UTRA physical layer aspects (Release 9)," March 2010.

[28] S. Kumar, I. Z. Kovacs, G. Monghal, K. I. Pedersen, and P. E. Mogensen, "Performance evaluation of 6-sector-site deployment for downlink UTRAN long term evolution," in *Proc. of IEEE 68th Vehicular Technology Conference, VTC 2008-Fall.*, pp. 1-5, 2008. Article (CrossRef Link)

[29] D. Lopez-Perez, A. Valcarce, G. d. l. Roche, and J. Zhang, "OFDMA femtocells: A roadmap on interference avoidance," *IEEE Communications Magazine*, vol. 47, no.9, pp. 41-48, 2009. Article (CrossRef Link)

[30] Z. Xu, G. Y. Li, C. Yang, and X. Zhu, "Throughput and optimal threshold for FFR schemes in OFDMA cellular networks," *IEEE Transactions on Wireless Communications*, vol. 11, no.8, pp. 2776-2785, 2012. Article (CrossRef Link)

[31] M. Maqbool, P. Godlewski, M. Coupechoux, and J.-M. Kélif, "Analytical performance evaluation of various frequency reuse and scheduling schemes in cellular OFDMA networks," *Performance Evaluation*, vol. 67, no. 4, pp. 318-337, 2010. Article (CrossRef Link)

[32] H. Cramér, *The elements of probability theory and some of its applications*. New York: John Wiley and Sons 1955. Article (CrossRef Link)

[33] S. M. Cheng, W. C. Ao, F. M. Tseng, and K. C. Chen, "Design and analysis of downlink spectrum sharing in two-tier cognitive femto networks," *IEEE Transactions on Vehicular Technology*, vol. 61, no. 5, pp. 2194-2207, 2012. Article (CrossRef Link)
[34] V. M. Daniel Zwillinger *Tables of integrals, sums, series, and products (Eigth Edition)*. Nauka, Moscow: Acadmic Press, 2014. Article (CrossRef Link)

Sani Umar Abdullahi received his B.Eng. degree in Electrical Engineering from Ahmadu Bello University Zaria, Nigeria in 2008 and an M.S. degree in Mobile and Satellite Communications from the Centre for Communications and Systems Research (CCSR) of University of Surrey in 2009. He is currently pursuing a Ph.D. degree with the School of Computer and Communications Engineering, University of Science and Technology (USTB), Beijing, China. His research area interests include Heterogeneous Networks, Hybrid Satellite-Terrestrial Systems, Stochastic Geometry applications in wireless networks, millimeter wave communications and recently 5G systems.

Jian Liu received his B.S. degree in Automatic Control Theory and Applications from Shandong University, China, in 2000, and the Ph.D. degree in School of Information Science and Engineering from Shandong University in 2008. He is currently an associate professor of University of Science and Technology (USTB), Beijing, China. His research interests include cognitive radio networks, mobile mesh networks, and LTE-A.

Seyed Alireza Mohadeskasaei received his BS and MS degrees in Electronics Engineering from the School of Electronic Engineering, Islamic Azad University, Najafabad branch, Iran in 2003 and 2005 respectively. He is currently pursuing a PhD degree with School of Computer and Communications Engineering, University of Science and Technology (USTB), Beijing, China. His research interests include; modeling and simulation of RF systems, wide band power amplifiers, millimeter wave networks and energy efficiency in mobile and ad-hoc networks